g-B_3N_3C: a novel two-dimensional graphite-like material

J. Y. Li, D. Q. Gao, X. N. Niu, M. S. Si,* and D. S. Xue†

Key Laboratory for Magnetism and Magnetic Materials of the Ministry of Education, Lanzhou University, Lanzhou 730000, China

(Dated: November 8, 2012)

Abstract

A novel crystalline structure of hybrid monolayer hexagonal boron nitride (BN) and graphene is predicted by means of the first-principles calculations. This material can be derived via boron or nitrogen atoms substituted by carbon atoms evenly in the graphitic BN with vacancies. The corresponding structure is constructed from a BN hexagonal ring linking an additional carbon atom. The unit cell is composed of 7 atoms, 3 of which are boron atoms, 3 are nitrogen atoms, and one is carbon atom. It behaves a similar space structure as graphene, which is thus coined as g-B_3N_3C. Two stable topological types associated with the carbon bonds formation, i.e., C-N or C-B bonds, are identified. Interestingly, distinct ground states of each type, depending on C-N or C-B bonds, and electronic band gap as well as magnetic properties within this material have been studied systematically. Our work demonstrates practical and efficient access to electronic properties of two-dimensional nanostructures providing an approach to tackling open fundamental questions in bandgap-engineered devices and spintronics.

PACS numbers: 73.22.Pr, 75.70.Ak, 78.67.Wj

I. INTRODUCTION

Two-dimensional (2D) nanomaterials, such as graphene and monolayer hexagonal boron nitride (h-BN), are expected to play a key role in future nanotechnology as well as to provide potential applications in next-generation electronics. Recently, novel hybrid structures consisting of a patchwork of BN and C nanodomains (BNC) was synthesized through the use of a thermal catalytic chemical vapour deposition method[1]. This finding immediately has attracted a great deal of research interest[2–4], given it demonstrating a hitherto efficient route to tune the band gaps of these 2D materials.

It is well known that the perfect hexagonal and planar structure of BNC largely depends on the well matching between BN and C domains. However, it is indeed an outstanding challenge as BN and C phases are naturally immiscible in 2D[1]. This explains why Ci *et al.*[1] could observe some wrinkles in atomic force microscopy (AFM) image. Such mutual contradiction mainly originates from the domain boundary effect and the staggered potentials of B and N atoms in BNC, which doubtlessly affects their continuous tunable electronic energy gaps. It has been confirmed in the related theoretical calculations[5–9] where the band gaps behave a strong oscillation feature.

The X-ray photoelectron spectroscopy (XPS) of BNC measured in the work from Ci *et al.*[1] shows two additional types of C bonding configurations, which correspond to the C-B and C-N bonds with the bonding energies of around 188.4 and 398.1 eV, respectively. This feature means that two inequivalent C bonding types, i.e., C-B or C-N bonds, must be present in the boundaries of the hybridized BN and C domains, which have a significant effect on determining the local structures and subsequently vary the electronic properties in this system. For example, the transport channels behave a robust characteristic gap when the topological index changes sign of the valley Hall effect[3]. In addition, both Raman D band at 1,360 cm^{-1} and D$'$ band at 1,620 cm^{-1} are also observed in BNC[1], which were attributed to the lattice disorder or the finite crystal size. This lattice disorder effect might directly introduce vacancies to these 2D hexagonal system[10–12], which is also true in BNC as shown in Fig. 2a of Ref.[1].

For the planar BNC structure, although the larger domains would be preferred to decrease the total domain interfacial energy, the randomly distributed hybrid domains, the immiscible phases as well as the induced vacancies must result in various complex structures

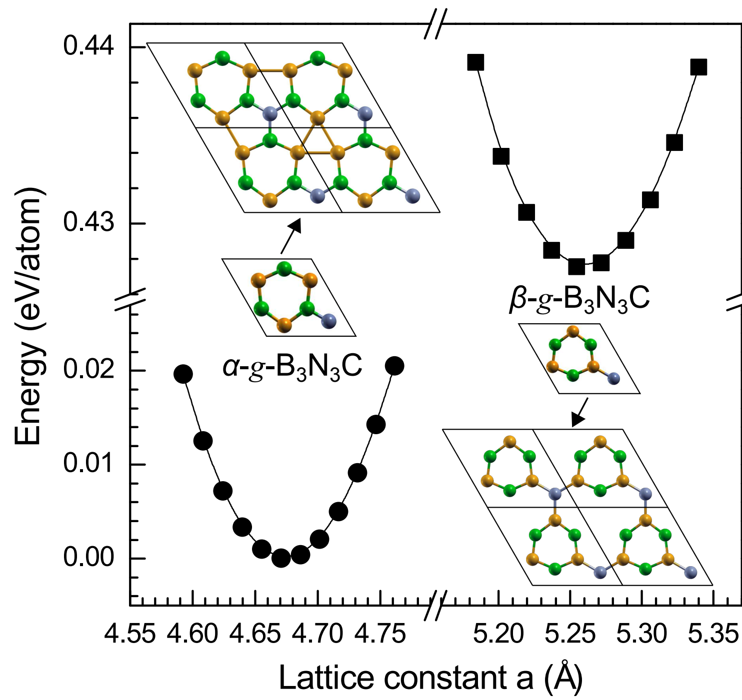

FIG. 1. The total energy per atom as a function of lattice constant a for g-B_3N_3C. Yellow, green, and gray balls represent B, N, and C atoms, respectively. Their respective 2×2 supercells are also given nearby.

of BNC[13–16]. As an immediate consequence is the largely inaccessible synthesis of expected BNC in experiments[17], which next hinders realization of bandgap-engineered applications in actual devices. In this endeavour, exploring the structures and electronic properties associated with C bonds formation in BNC that contain C-N or C-B bonds is an interesting topic that must be addressed before widespread synthetic applications. Thus, a simple model of BNC where the C bonds play a crucial role must be considered again. More importantly, a deep theoretical understanding, which originally was concealed behind the complex hybridized structures, is imperative.

Here we report such a simple model of BNC may be just the graphitic B_3N_3C (g-B_3N_3C), which is a perfect 2D monolayer graphite-like structure as shown in Fig. 1. As mentioned above, C atom can bond to B and N atoms. Therefore, two topological types of g-B_3N_3C are easily deduced. One is the α-g-B_3N_3C related to the the higher bonding energy of C-N bond, while the other one is the β-g-B_3N_3C constructed based on the lower bonding energy of C-B bond. It can be seen that such a material is essentially C-doped graphitic

BN (g-BN) with vacancies[11]. The substitution of the N/B atom with a C atom in g-BN with the B/N vacancy will yield the α/β-g-B_3N_3C structure. The interactions among the C atoms and/or vacancies as well as the C bonding types (C-B and C-N bonds) in g-B_3N_3C significantly alter its electronic properties. To explore this effect, standard density functional theory with different functionals (see the following discussion) calculations have been carried out for this predicted material. Remarkably, such material displays two distinct electronic structure properties: α-g-B_3N_3C is a semiconductor, while β-g-B_3N_3C behaves metallic and leads to a magnetic ground state.

This paper is arranged as follows: In the second section, we present the computational method used in this work, followed by electronic band gap in α-g-B_3N_3C and magnetism in β-g-B_3N_3C in the third section. We then conclude this paper in the fourth section.

II. COMPUTATIONAL METHOD

For structural optimization, we employed density functional theory with the generalized gradient approximation (GGA) of Perdew-Burke-Ernzerhof (PBE)[18] for the exchange-correlation (XC) potential within the projector augmented wave method as implemented in VASP[19]. An all-electron description, the projector augmented wave method, is used to describe the electron-ion interaction. The cutoff energy for plane waves is set to be 500 eV, and the vacuum space is at least 15 Å, which is large enough to avoid the interaction between periodical images. A 7×7×1 Monkhorst-Pack grid is used for the sampling of the Brillouin zone during geometry optimization. All the atoms in the unit cell were allowed to relax, and the convergence of force is set to 0.01 eV/Å. Additionally, spin polarization is turned on during the relaxation processes. All other calculations of accurate electronic properties were performed using the full-potential linearized augmented plane-wave (FLAPW)[20] method as implemented in the WIEN2k code[21]. It is well known that different XC potentials can lead, depending on the studied materials and properties, to results which are in very bad agreement with experiment, e.g., for the band gap of semiconductors and insulators which is severely underestimated or even absent[22]. For this reason, the modified Becke and Johnson (MBJ)[23,24] potential in the framework of local-density approximation (LDA)[25,26] is taken to calculate the band gap of α-g-B_3N_3C, while the magnetism in β-g-B_3N_3C is described by the PBE (the standard GGA for materials) potential.

III. RESULTS AND DISCUSSION

A. Electronic band gap in α-g-B_3N_3C

Figure 1 plots the total energy per atom against the lattice constant a (the lattice constant c is fixed) for g-B_3N_3C. It can be seen that the total energy of g-B_3N_3C as a function of lattice constant a has a single minimum, meaning that the geometrical structure would be stable. Particularly, the charge population analysis reveals that the electron density around the C-N bond in α-g-B_3N_3C is much higher than that on the C-B bond in β-g-B_3N_3C, showing that the C-N bond is relatively strong, which is also consistent with the experimental results[1]. This strong interaction between C and N atoms in α-g-B_3N_3C directly results in a short C-N bond length (see following), and can balance the strain of the monolayer graphite-like structure. Thereby α-g-B_3N_3C could be a more thermodynamically stable topological phase against β-g-B_3N_3C, which has a lower total energy of around 0.43 eV/atom compared with β-g-B_3N_3C.

To explore further the mechanical stability of α-g-B_3N_3C, the optimized lattice constant a = 4.67 Å is first obtained, as depicted in the left panel of Fig. 1. Importantly, the C-N bond length converged to 1.31 Å, considerably reduced from the typical bond lengths 1.37-1.48 Å in the related materials[27]. This strongly suggests that the nature of the higher binding energy of C-N bond[1], which also influences the B-N bonding and extends its length. The obtained B-N bond length is 1.48 Å, which is slightly bigger than the value of 1.45 Å in h-BN. The calculated partial density of states (PDOS) is shown in Fig. 2. The valence band is dominated by B p and C p states, while the conduction band is only dominated by B p states. There one can find that the majority of C p states to be semicore lying 6-9 eV below the Fermi level. These states interact with those comprising the valence band with the same symmetry. As a result there is a small admixture of C p and N p states close to the Fermi level. However, in α-g-B_3N_3C one finds significant admixture of C p and N p states in the semicore energy window with 6-9 eV below the Fermi level. This suggests that the C p-N p interaction in semicore region contribution to the C-N bonding is significantly more important in α-g-B_3N_3C than the C p-N p interaction close to the Fermi level.

Now, let us look at the band structures of α-g-B_3N_3C, as given in Fig. 3. It explicitly demonstrates that all three XC potentials give similar band structures. The highest occupied

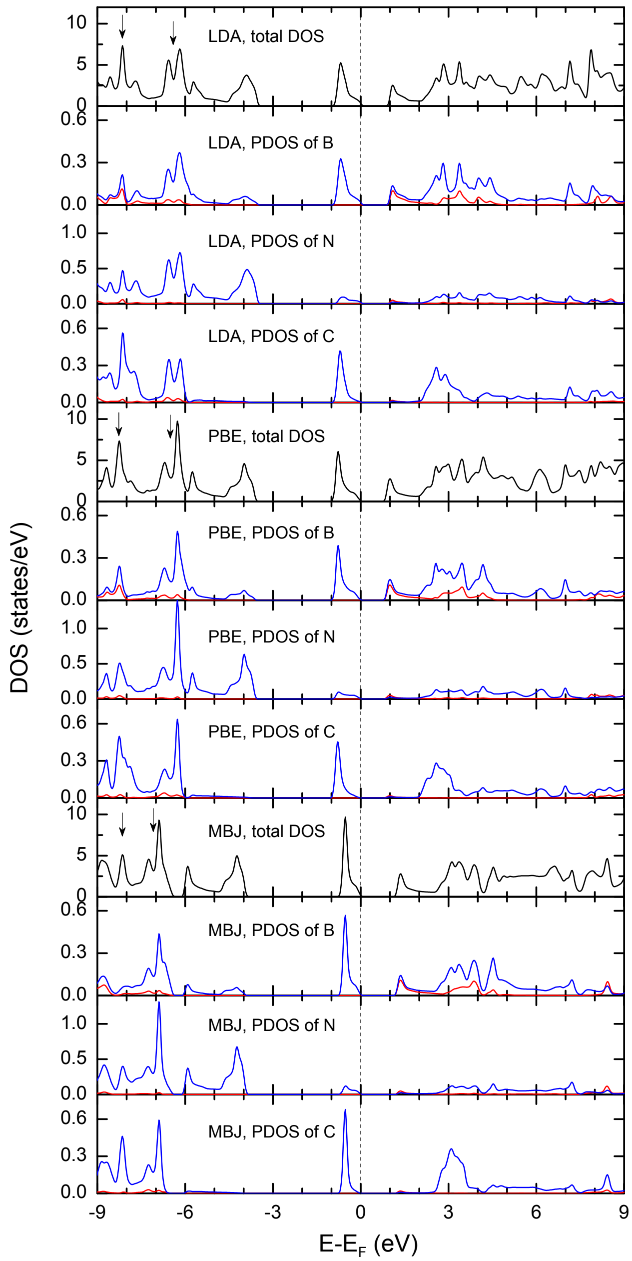

FIG. 2. Total and partial DOS of α-g-B_3N_3C for three XC potentials LDA, PBE, and MBJ. The vertical dotted line denotes the Fermi level, and also indicates end of the fundamental band gap which starts at $E - E_F = 0$ eV. The black, blue, and red lines correspond to the total, p, and s DOS, respectively.

crystalline orbitals (HOCOs) are located at the K point of the reciprocal space, while the lowest unoccupied crystalline orbitals (LUCOs) appear at the M point. This leads to an indirect-band-gap semiconductor. To obtain the band gap more accurately [see Fig. 3(c)],

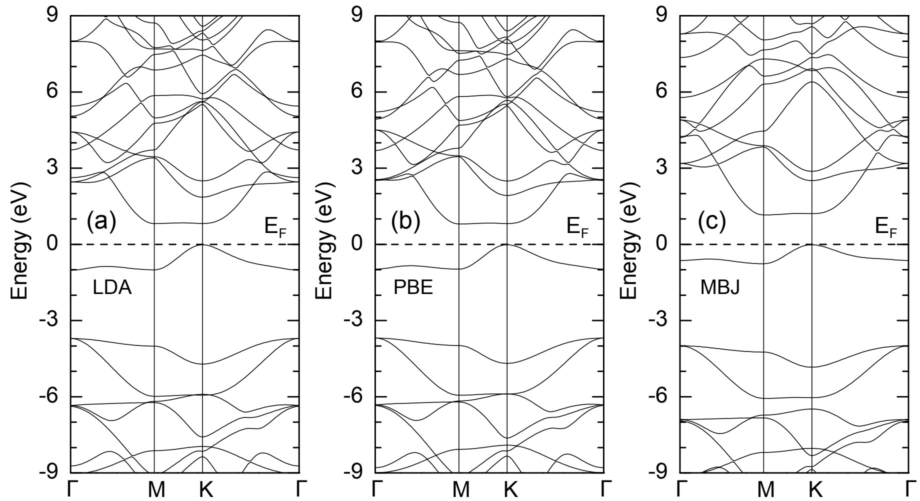

FIG. 3. Calculated band structures for α-g-B_3N_3C model with the three XC potentials LDA (a), PBE (b), and MBJ (c).

the MBJ XC functional is used[23,24]. The band gap of α-g-B_3N_3C within MBJ is obtained to be 1.22 eV, which nicely locates the middle region between 0.59 and 1.80 eV for the BNC samples with 12.5% and 50% C contents, respectively[4]. Note that the C content in α-g-B_3N_3C is 25%. In the experiments[1], the absorption edges are redshifted as the C concentrations increase, which shows a tunable mechanism of optical band gap in actual applications. By comparing with Ref.[1] where BNC with around 65% C concentration shows an optical bandgap of 1.62 eV, we infer that such a higher energy absorption edge (take into account the band gap of 1.22 eV in our case with 25% C concentration) arises from the formation of individual BN and graphene domains. In this way, the even distribution of C in BNC systems might serve as a good guide to find alternative solutions to existing bandgap-engineered applications. Future researches can test this prediction directly.

In addition, the band gaps based on the LDA and PBE methods are equal to 0.83 eV [see Figs. 3(a) and (b)]. The relative band gap correction from MBJ with respect to LDA, $\mathcal{R} = (\Delta_{\mathrm{MBJ}} - \Delta_{\mathrm{LDA}})/\Delta_{\mathrm{MBJ}}$ with $\Delta_{\mathrm{MBJ/LDA}}$ being the band gap, is about 32%. We can see that our calculated $\mathcal{R}$ for α-g-B_3N_3C (shows an excellent agreement with the 16 *sp* semiconductors) lies within the range 16.0%-100.0% (see Table 1 for details). The correction value is particularly very close to that in BN (25%), GaN (42%), AlP (37%), and AlN (25%). This finding is not surprised because the listed 4 solids have at least one element close to that of α-g-B_3N_3C in the periodic table of elements. It means the similar chemical circumstances

TABLE I. The band gaps (in eV) and the relative band gap correction $\mathcal{R}$ (%) of 16 *sp* semiconductors and the predicted α-g-B_3N_3C. The theoretical and experimental band gaps of the 16 *sp* semiconductors are directly taken in[24].

Solid	LDA	MBJ	$\mathcal{R}$	Expt.
C	4.11	4.93	16.6	5.48
Si	0.47	1.17	59.8	1.17
Ge	0.00	0.85	100.0	0.74
LiF	8.94	12.94	30.9	14.20
LiCl	6.06	8.64	29.9	9.40
MgO	4.70	7.17	34.4	7.83
ScN	-0.14	0.90	115.6	0.90
SiC	1.35	2.28	40.8	2.40
BN	4.39	5.85	25.0	6.25
GaN	1.63	2.81	42.0	3.20
GaAs	0.30	1.64	81.7	1.52
AlP	1.46	2.32	37.1	2.45
ZnS	1.84	3.66	49.7	3.91
CdS	0.86	2.66	67.7	2.42
AlN	4.17	5.55	24.9	6.28
ZnO	0.75	2.68	72.0	3.44
α-g-B_3N_3C	0.83	1.22	32.0	–

in these materials can be well described by the same XC functionals. This underlyingly confirms our prediction validity and the α-g-B_3N_3C might be carried out experimentally.

From Fig. 2, which shows the DOS of α-g-B_3N_3C, we can see that the effect of the MBJ potential is to shift up (with respect to LDA/PBE) the unoccupied B $2s$ and $2p$ states. Here, three major differences between the LDA/PBE and MBJ methods can be extracted. (a) Another obvious effect of MBJ potentials is to shift down the middle of the valence band at around -4.0 eV. (b) The hybridization of s and p states of dominant B $2s$ and other atoms $2p$ states at the bottom of the valence band is very strong in MBJ calculations

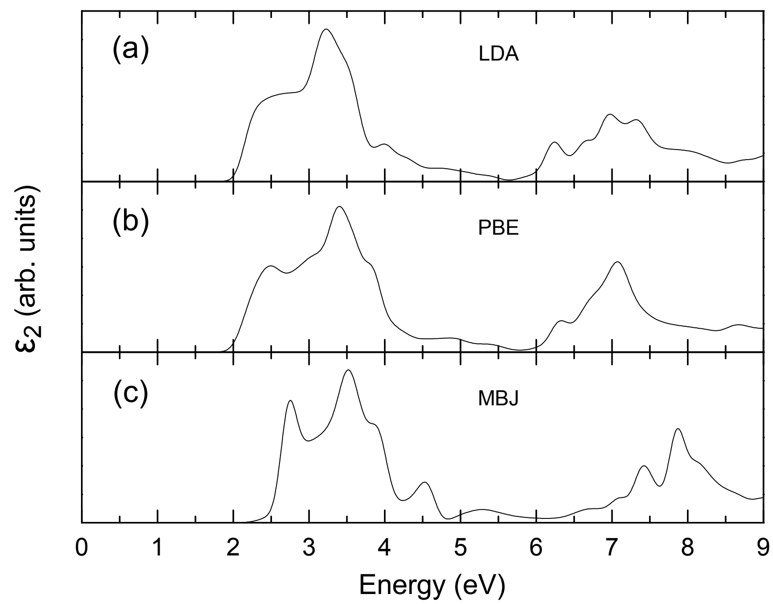

FIG. 4. The optical absorption expressed by the imaginary part of the dielectric tensor ε_2 for α-g-B_3N_3C. The imaginary part of the dielectric tensor is averaged for four different directions. Three XC potentials including LDA (a), PBE (b), and MBJ (c) are shown in calculations.

(denoted as down arrows in Fig. 2). (c) The correction character of α-g-B_3N_3C is much more pronounced with the MBJ than with the LDA/PBE, which narrows the valence band just below the Fermi level. We would like to stress that the MBJ potentials open a band gap of 0.39 eV in the α-g-B_3N_3C model compared to the result of LDA, which is consistent with the orbital-dependent potentials principle[24].

The optical absorption spectrum for α-g-B_3N_3C within MBJ potentials [see Fig. 4(c)] shows a big absorption packet with two adjacent peaks in the range of 2.5-5.0 eV, which originates from the band structure as shown in Fig. 3(c). As an indirect band gap material, the transition from the K to Γ point is very weak as the momentum conservation rule is not satisfied here, and thus the corresponding characteristic photoluminescence in the optical absorption spectrum can be negligible. This is also true in our case α-g-B_3N_3C. The first peak corresponds to the direct band gap transition at the M point. The second peak comes from the larger direct gap from higher energy states located at the Γ point. More importantly, these two peaks are not separated distinctly. This feature can be attributed to the even distribution of C atoms in α-g-B_3N_3C as mentioned above, which behaves a different formation mechanism compared with the hybrid BNC in experiment[1].

Correction effects were taken into account by adding a LDA correction potential in MBJ[24]. This important physical effect opens an additional band gap through mimicing very well the behavior of orbital-dependent potentials and causes a rigid blueshift of the absorption spectrum compared with the LDA/PBE curves as shown in Fig. 4. This explains the excellent qualitative agreement of the hybrid exchange potential optical absorption spectrum seen in Fig. 4, due to a compensation of significant errors within the standard DFT methods.

B. Magnetism in β-g-B_3N_3C

The predicted structure of β-g-B_3N_3C is shown in the right panel of Fig. 1. The lattice constant of β-g-B_3N_3C is obtained to be 5.26 Å as shown in Fig. 1. The results show that the equilibrium value $d_{\mathrm{BC}} = 1.52$ Å, which is close to the value of graphite-like BC_3, namely, 1.55 Å[28]. It is to be noticed that all the equilibrium values d_{BN} in α-g-B_3N_3C are equal to 1.42 Å, which is slightly less than the value of 1.45 Å in pristine BN sheet. This implies the stronger B-N bonds formed in β-g-B_3N_3C. Our calculations show that the β-g-B_3N_3C leads to a ground state with a magnetic moment of 0.68 μ_{B}. The nonmagnetic state is 0.07 eV higher than this ground state.

From the band structures we see that although both the pristine BN sheet and graphene are nonmagnetic, the β-g-B_3N_3C model can be spin polarized. It is necessary to discuss magnetism in more detail from its electronic structures. Figures 5(a)-(c) present the band structure and spin-resolved total density of state (TDOS). Remarkably, two bands cross the Fermi level [black and red circles in Fig. 5(a)], and make the Fermi energy level occupied completely along the entire high-symmetry lines. In contrast, the spin-down one does not possess such a strongly localization feature, just one band (black circles) crosses the Fermi level monolithically as shown in Fig. 5(c). The calculated magnetic moment in β-g-B_3N_3C should originate from this asymmetric spin-dependent localization. The corresponding strong spin splitting can be further confirmed from TDOS as shown in Fig. 5(b). In addition, close examination of the top valence bands [see Fig. 6(a)] indicates that the strong localization mainly comes from the $2p$ atomic orbitals of C and N atoms. Here we also show that the Fermi surfaces of β-g-B_3N_3C in the first Brillouin zone. The unique feature of Fermi surface almost parallel to the high-symmetry lines [see Figs. 5(d)-(f)] is the direct manifestation of the bands near the Fermi level in Figs. 5(a) and 5(c).

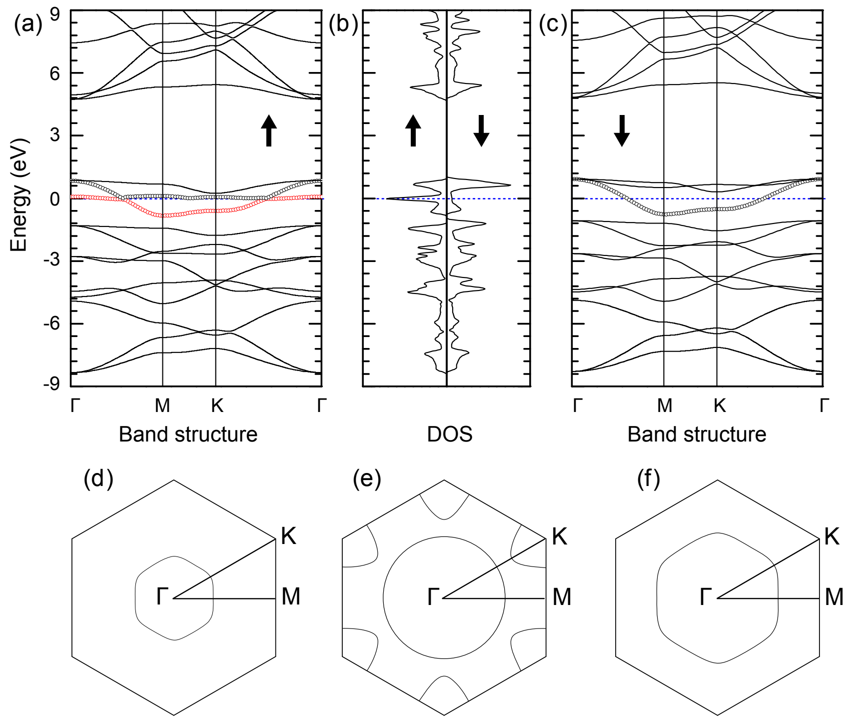

FIG. 5. (a)-(c) Band structures and spin-resolved TDOS for β-g-B_3N_3C. The dotted line indicates the Fermi level. The arrow denotes the spin polarization direction: up for spin up and down for spin down. (d)-(f) Fermi surfaces drawn in the first Brillouin zone and the corresponding high-symmetry points. (d) and (e) for spin up and (f) for spin down.

It should be notice that such magnetism is induced without transition metals and without external perturbations, so that β-g-B_3N_3C behaves as the first, theoretically predicted, metal-free magnetic material in hybrid BNC system. Apparently, our finding points out a new direction for further related experimental investigations in spintronics.

We now address the possibility to magnetism origin in β-g-B_3N_3C. Based on the orbital-resolved density of state as shown in Fig. 6(a), the magnetic moment are mainly ascribed to the $2p$ orbitals of C and three N atoms. The spin polarization of C atom offers a magnetic moment of 0.18 μ_B. 0.18 μ_B of total magnetic moment are shared equally by the $2p$ orbitals of three N atoms. The remaining magnetic moments distribute evenly in the interstitial region among N atoms. This is conceivable, because β-g-B_3N_3C, if compared with other BNC systems, has large interspaces between N atoms [see the 2×2 supercell in Fig. 1 or Fig. 6(b)]. The remarkable feature is that the equilibrium surface density of β-g-B_3N_3C is around 1.27 times larger than α-g-B_3N_3C. Owing to the large interspaces between atoms,

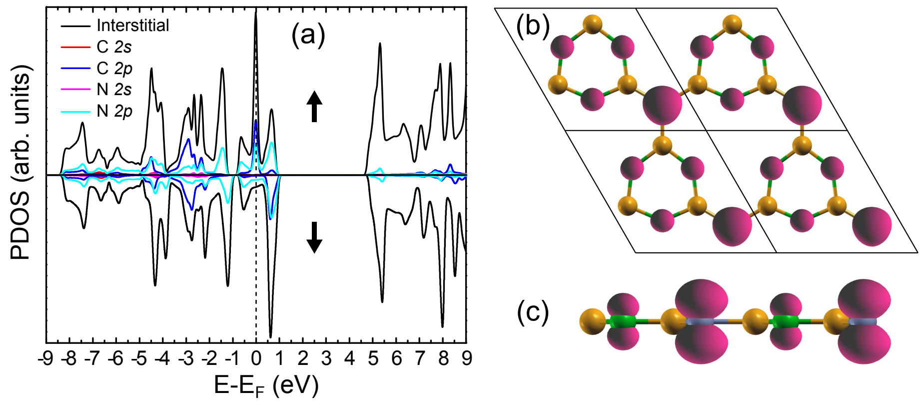

FIG. 6. (a) PDOS on the interstitial region and on the $2s$ and $2p$ orbitals of C and N atoms in β-g-B_3N_3C. (b) The 3D iso-surface plot of spin density for the 2×2 supercell at the value of 0.04 e/$Å^3$: (c) A side view of spin density corresponding to (b).

the hydrogen storage in β-g-B_3N_3C may be expected[29]. The detailed description of hydrogen storage related to β-g-B_3N_3C is beyond the scope of this work.

Concerning the special carbon atom in β-g-B_3N_3C, the counting of four valence electrons is as follows: Three electrons participate in the sp^2 hybrid orbital, which forms a planar structure. The remaining one electron is then redistributed in the whole unit cell due to the enhanced B-N covalent bond (with shorter bond length compared with the value in pristine h-BN), which makes the magnetic properties more complicated. From the fourth electron, only 18 percent of the electron still fill the π-orbital of C atom and contribute a magnetic moment of 0.18 μ_B. This is in fairly good agreement with theoretical description of the π-orbital state to the local magnetic moment $\sim$0.3 μ_B in the graphene-like systems[30,31]. Around 32% of the fourth electron mainly reside at the interstitial region, which play a crucial role in β-g-B_3N_3C as: (a) Enhance the B-N covalent bond. (b) Provide the main interstitial magnetic moment of 0.32 μ_B. (c) Promote the $2p_z$ of N atom spin polarized slightly with a magnetic moment of 0.06 μ_B per N atom. The remaining of the fourth electron act as the conduction electrons and make the system metallic, which dominate the mechanism of ferromagnetic ordering in β-g-B_3N_3C. In the case of β-g-B_3N_3C, we can see that the electron spin at the localized π-orbital state of C and N atoms, as well as the interstitial region compel two energy bands localized strictly along the entire high-symmetry lines, i.e., the Γ-M-K-Γ line [see Fig. 5(a)]. Thus, the RKKY interaction[32,33] among the magnetic sites through the residual conduction electrons forms a spin ordering in these orbitals, which is the physical

origin of ferromagnetism in β-g-B_3N_3C. Figures 6(b) and 6(c) respectively plot the top and side views of the 3D iso-surfaces for net magnetic charge density in xy plane. This finding is insightful and three major points deserve comment: (a) The C site is more spin polarized as compared with each N site. (b) The dumbbell-like magnetic moment distribution along z direction implies the $2p_z$ orbital becomes partially filled with one spin-up electron. (c) The induced moments are ferromagnetic coupled between the N and C sites based on the RKKY exchange interaction model as mentioned above.

IV. CONCLUSIONS

In summary, we have predicted a novel crystalline material g-B_3N_3C, which displays two distinct electronic properties where the selective bonding type of C atom is a key parameter for future industrial processes. α-g-B_3N_3C is a semiconductor, while β-g-B_3N_3C behaves metallic and holds a magnetic moment of 0.68 μ_B. Importantly, compared with the hybrid BNC, g-B_3N_3C is proposed to have a simple structure, which can be applied in various fields due to its unique properties.

ACKNOWLEDGMENTS

This work was supported by the National Basic Research Program of China under No. 2012CB933101. This work was also supported by the National Science Foundation of China (NSFC) under No. 10804038, 11034004, and 50925103, and the Fundamental Research Fund for the Central Universities and Physics and Mathematics of Lanzhou University. We acknowledge part of the work as done on National Supercomputing Center in Shenzhen.

* sims@lzu.edu.cn

† xueds@lzu.edu.cn

[1] L. Ci, L. Song, C. Jin, D. Jariwala, D. Wu, Y. Li, A. Srivastava, Z. F. Wang, K. Storr, L. Balicas, F. Liu, and P. M. Ajayan, Nat. Mater. **9**, 430 (2010).

[2] A. Rubio, Nat. Mater. **9**, 379 (2010).

[3] J. Jung, Z. Qiao, Q. Niu, and A. H. MacDonald, Nano Lett. **12**, 2936 (2012).

[4] M. Bernardi, M. Palummo, and J. C. Grossman, Phys. Rev. Lett. **108**, 226805 (2012).

[5] J. Li and V. B. Shenoy, Appl. Phys. Lett. **98**, 013105 (2011).

[6] K. Lam, Y. Lu, Y. P. Feng, and G. Liang, Appl. Phys. Lett. **98**, 022101 (2011).

[7] G. Seol and J. Guo, Appl. Phys. Lett. **98**, 143107 (2011).

[8] J. da Rocha Martins and H. Chacham, ACS Nano **5**, 385 (2010).

[9] A. K. Manna and S. K. Pati, J. Phys. Chem. C **115**, 10842 (2011).

[10] P. O. Lehtinen, A. S. Foster, A. Ayuela, A. Krasheninnikov, K. Nordlund, and R. M. Nieminen, Phys. Rev. Lett. **91**, 017202 (2003).

[11] M. S. Si and D. S. Xue, Phys. Rev. B **75**, 193409 (2007).

[12] M. S. Si, J. Y. Li, H. G. Shi, X. N. Niu, and D. S. Xue, Europhys. Lett. **86**, 46002 (2009).

[13] J. M. Pruneda, Phys. Rev. B **85**, 045422 (2012).

[14] M. S. C. Mazzoni, R. W. Nunes, S. Azevedo, and H. Chacham, Phys. Rev. B **73**, 073108 (2006).

[15] A. Enyashin, Y. Makurin, and A. Ivanovskii, Carbon **42**, 2081 (2004).

[16] S. Dutta and S. K. Pati, J. Phys. Chem. B **112**, 1333 (2008).

[17] W. Han, L. Wu, Y. Zhu, K. Watanabe, and T. Taniguchi, Appl. Phys. Lett. **93**, 223103 (2008).

[18] J. P. Perdew, K. Burke, and M. Ernzerhof, Phys. Rev. Lett. **77**, 3865 (1996).

[19] G. Kresse and J. Furthmüller, Comp. Mater. Sci. **6**, 15 (1996); Phys. Rev. B **54**, 11169 (1996).

[20] G. K. H. Madsen, P. Blaha, K. Schwarz, E. Sjöstedt, and L. Nordström, Phys. Rev. B **64**, 195134 (2001).

[21] P. Blaha, K. Schwarz, G. K. H. Madsen, D. Kvasnicka, and J. Luitz, *WIEN2k, An Augmented Plane Wave + Local Orbitals Program for Calculating Crystal Properties* (K. Schwarz, Techn. Universität Wien, Austria, 2001).

[22] J. Heyd, J. E. Peralta, G. E. Scuseria, and R. L. Martin, J. Chem. Phys. **123**, 174101 (2005).

[23] A. D. Becke and E. R. Johnson, J. Chem. Phys. **124**, 221101 (2006).

[24] F. Tran and P. Blaha, Phys. Rev. Lett. **102**, 226401 (2009).

[25] W. Kohn and L. J. Sham, Phys. Rev. **140**, A1133 (1965).

[26] J. P. Perdew and Y. Wang, Phys. Rev. B **45**, 13244 (1992).

[27] arXiv:0804.2488v3 [physics.gen-ph].

[28] D. Tomanek, R. M. Wentzcovitch, S. G. Louie, and M. L. Cohen, Phys. Rev. B **37**, 3134 (1988).

[29] R. E. Mapasha, A. M. Ukpong, and N. Chetty, Phys. Rev. B **85**, 205402 (2012).

[30] K. Tada, J. Haruyama, H. X. Yang, M. Chshiev, T. Matsui, and H. Fukuyama, Phys. Rev. Lett. **107**, 217203 (2011).

[31] H. Lee, Y. W. Son, N. Park, S. Han, and J. Yu, Phys. Rev. B **72**, 174431 (2005).

[32] P. O. Lehtinen, A. S. Foster, A. Ayuela, A. Krasheninnikov, K. Nordlund, and R. M. Nieminen, Phys. Rev. Lett. **91**, 017202 (2003).

[33] P. Bruno and C. Chappert, Phys. Rev. B **46**, 261 (1992).